PNAS RESEARCH ARTICLE | MICROBIOLOGY OPEN ACCESS

The inhibitory mechanism of a small protein reveals its role in antimicrobial peptide sensing

Shan Jiang[a,b], Lydia C. Steup[a,b], Charlotte Kippnich[a,b], Symela Lazaridi[c,d], Gabriele Malengo[a,b], Thomas Lemmin[c], and Jing Yuan[a,b,1]

Edited by Gisela Storz, National Institute of Child Health and Human Development, Bethesda, MD; received June 7, 2023; accepted September 6, 2023

A large number of small membrane proteins have been uncovered in bacteria, but their mechanism of action has remained mostly elusive. Here, we investigate the mechanism of a physiologically important small protein, MgrB, which represses the activity of the sensor kinase PhoQ and is widely distributed among enterobacteria. The PhoQ/PhoP two-component system is a master regulator of the bacterial virulence program and interacts with MgrB to modulate bacterial virulence, fitness, and drug resistance. A combination of cross-linking approaches with functional assays and protein dynamic simulations revealed structural rearrangements due to interactions between MgrB and PhoQ near the membrane/periplasm interface and along the transmembrane helices. These interactions induce the movement of the PhoQ catalytic domain and the repression of its activity. Without MgrB, PhoQ appears to be much less sensitive to antimicrobial peptides, including the commonly used C18G. In the presence of MgrB, C18G promotes MgrB to dissociate from PhoQ, thus activating PhoQ via derepression. Our findings reveal the inhibitory mechanism of the small protein MgrB and uncover its importance in antimicrobial peptide sensing.

small protein | sensor kinase | antimicrobial peptide | bacteria signaling | two-component system

Significance

Small proteins have high prevalence, vast diversity, and primarily regulatory functions in biological processes across all domains of life. However, their mechanisms of action remain largely elusive. In this study, we investigate the mechanism of the small protein, MgrB. It interacts with the sensor kinase PhoQ, rearranges its conformation, represses its kinase activity, and regulates bacterial response to environmental changes. In particular, for antimicrobial peptides, MgrB is required for bacteria to have a selective response to this host-exclusive stimulus. Our findings underline the importance of a small protein in bacterial fitness and drug resistance and provide a molecular basis for engineering peptide-based regulators.

Small proteins are defined by their short sequences (usually < 50 aa) and their direct synthesis via ribosomal translation. An increasing number of small proteins have been identified in individual species in all domains of life and complex biological communities, suggesting a high prevalence and vast diversity in biological systems (reviewed in refs. 1–4). Many of these small proteins (~30%) are located in the cell membrane or have been predicted to be located there (e.g., refs. 5 and 6). Although only a few detailed studies of small membrane proteins have been conducted, results show that small proteins may target larger proteins and the lipid bilayer, regulating protein function, abundance, and changing membrane properties, demonstrating their predominant role as regulators in the lipid bilayer (reviewed in ref. 7).

The membrane located PhoQ sensor kinase, a master regulator of a bacterial virulence program, detects host-associated stimuli (review in ref. 8), such as cationic antimicrobial peptides (CAMPs) (9), mild acidic pH (10, 11), increased osmolarity (12), biliary unsaturated long-chain fatty acids (13), and magnesium limitation (14). Three small membrane proteins have been identified to control PhoQ activity via direct protein–protein interactions. In *E. coli,* MgrB (47aa) and SafA (65aa) modulate PhoQ activity, with MgrB acting as an inhibitor and SafA as an activator (15, 16). Deletion of *mgrB* or *safA* has physiological consequences, resulting in a cell division block under magnesium starvation or lowered acid resistance, respectively (17, 18). In *Salmonella enterica* serovar Typhimurium, a species-specific small protein, UgtS (34 aa), was reported recently and shown to control the timing of virulence gene expression by preventing premature PhoQ activation when inside macrophages (19).

The PhoQ sensor kinase is found as a dimer on the bacterial inner membrane. It consists of a periplasmic, a transmembrane (TM), a HAMP, a DHp, and a catalytic ATP-binding domain. In the periplasmic domain, several molecular interactions are essential for the functional state of the PhoQ molecule. These include the central hydrogen bonding network (T48 D179 K186) in the PAS-fold (20–23), the intermonomeric salt bridge (D179-R50') (24), the membrane-facing acidic cluster (^{148}EDDDDAE), and the juxta-membrane region at the periplasm/inner-membrane interface (9, 23, 25). Mutations altering these molecular interactions change the conformation of the periplasmic domain and the sensitivity of PhoQ to magnesium, low pH, and/or CAMPs. Additionally, different stimuli may result in distinct conformational states of the periplasmic domain, at least in an in vitro setting. For example, the PhoQ periplasmic domain showed divergent NMR spectra in low pH compared to that in low magnesium conditions (10). Besides the periplasmic domain, the PhoQ transmembrane domain was shown to detect environmental

Author affiliations: [a]Max Planck Institute for Terrestrial Microbiology, 35043 Marburg, Germany; [b]Center for Synthetic Microbiology, 35043 Marburg, Germany; [c]Institute of Biochemistry and Molecular Medicine, Faculty of Medicine, University of Bern, 3012 Bern, Switzerland; and [d]Graduate School for Cellular and Biomedical Sciences, University of Bern, 3012 Bern, Switzerland

Author contributions: T.L. and J.Y. designed research; S.J., L.C.S., C.K., S.L., and J.Y. performed research; S.J., L.C.S., C.K., S.L., G.M., and J.Y. analyzed data; and S.J., T.L., and J.Y. wrote the paper.

The authors declare no competing interest.

This article is a PNAS Direct Submission.

[1]To whom correspondence may be addressed. Email: jing.yuan@synmikro.mpi-marburg.mpg.de.

This article contains supporting information online at https://www.pnas.org/lookup/suppl/doi:10.1073/pnas.2309607120/-/DCSupplemental.

Published October 4, 2023.

osmotic upshifts, where the transmembrane four-helix bundle adopts a more compact and kinase-active conformation (12).

Among the known PhoQ-regulating small proteins, MgrB is the most widely distributed PhoQ repressor in enterobacteria. In *Salmonella*, the deletion of *mgrB* was shown to affect its infection of macrophages and epithelial cells (26). In *Klebsiella pneumonia*, the disruption of the *mgrB* gene is the most prevalent among other chromosomal mutations in colistin-resistant strains (27). The expression of *mgrB* is PhoPQ dependent. Thus, the inhibitory function of MgrB provides negative feedback to the two-component system, resulting in a partial adaptation of *E. coli* to environmental changes (15, 28). MgrB is a bitopic inner membrane protein with a short cytosolic N terminus and a periplasmic C-terminal region (Fig. 1*A*). Two conserved cysteines (C28 and C39) in the periplasmic region were shown to be essential for MgrB function and suggested to form a disulfide bond (15). This disulfide bond was proposed to allow MgrB to act as a sensor for the redox state of the bacterial periplasm and create an entry point for redox sensing by the PhoQ/PhoP system (29). Besides the two cysteines, eight functionally essential residues were identified spread across the entire molecule (30). However, the mechanism of MgrB inhibiting PhoQ remained largely unclear.

In this study, we combined cross-linking approaches with functional assays and protein dynamic simulations to identify interactions between PhoQ and MgrB, probe MgrB-induced PhoQ conformational changes, and examine the impact of MgrB on PhoQ sensing environmental stimuli. We propose that the binding of MgrB i) changes the conformation of the linker region between PhoQ periplasmic and transmembrane domains, ii) rearranges the transmembrane four-helix bundle, and iii) initiates the translocation of the catalytic domain. MgrB interferes with PhoQ signaling, resulting in an overall lowered activity, but still allows PhoQ activation under low pH, osmotic upshift, and magnesium limitation. We further reveal that MgrB mediates PhoQ sensing antimicrobial peptides, enabling bacteria to have a selective response to this exclusively host-associated stimulus.

Results

Structural Predictions by AlphaFold2. We used AlphaFold2 multimer (31–33) to predict the structures of the PhoQ/MgrB complex as well as the individual component of the complex (Fig. 1 *B* and *C* and *SI Appendix*, Fig. S1). The overall prediction of structural elements agrees with previous experimental evidence. For example, the two conserved periplasmic cysteine residues (C28 and C39) in MgrB were positioned in close proximity in the models, structurally supporting the presence of a disulfide bond. In the PhoQ predictions, the PAS fold in the periplasmic domain, the HAMP, the DHp, and the cytosolic catalytic-ATP binding domains resembled the experimental results of these structural motifs (24, 34). Notably, the region connecting the periplasmic and TM domains and that connecting the HAMP and DHp domains showed a lower predicted local distance difference test (pLDDT) score (colored in yellow to green in *SI Appendix*, Fig. S1), indicating that these linker regions might have a higher capability of adopting different conformations. Unlike the asymmetric crystal structure of the PhoQ sensor domain (24), the AlphaFold2 predicted PhoQ dimer was symmetric, which likely represented only one of many conformations that PhoQ could adopt. In all five PhoQ/MgrB complex models (Fig. 1*B* and *SI Appendix*, Fig. S1), MgrB was placed in between the two PhoQ protomers, with the transmembrane helix parallel to the PhoQ TM helices and the C-terminal short helix (A40-W47) protruding away from PhoQ. The five predicted complex models had only minor differences regarding the positioning of MgrB. Because the PhoQ dimer was mostly symmetrical, AlphaFold2 randomly placed MgrB on one or the other side of the PhoQ dimer (*SI Appendix*, Fig. S1). When bound to PhoQ, MgrB showed a major conformational change in the region flanked by the two conserved cysteines (C28 and C39). This region had reduced helicity and rigidness and appeared as an extended flexible loop (Fig. 1*C*).

Disulfide Cross-Linking between MgrB and PhoQ TM Helices. Before AlphaFold was available, we used the disulfide cross-linking approach to identify the interacting residues in PhoQ and MgrB. We started with residue W20 in the MgrB TM helix, which was suggested to have direct contact with PhoQ (30). Sequence alignment of MgrB homologs from different bacterial species revealed both W and Y conserved at position 20 (*SI Appendix*, Fig. S2). The MgrB W20Y variant also showed strong inhibitory activity comparable to the wild type (*SI Appendix*, Fig. S2). Since both W and Y have an aromatic ring structure and a polar moiety, we predicted that the nature of the interactions at position 20 likely includes hydrophobic interactions and hydrogen bonding. Scanning through the sequence of the two PhoQ transmembrane helices, Y32 in TM1 appeared to be the optimal candidate to fulfill both types of interaction with MgrB W20.

To test this prediction with disulfide cross-linking, we constructed a PhoQ TM_Cys library and generated the MgrB C16A W20C variant, which has only one cysteine residue in the transmembrane helix. The Cys to Ala mutation at MgrB position 16 did not appear to have a functional effect (*SI Appendix*, Fig. S2*B*). However, the Trp to Cys mutation at position 20 significantly reduced MgrB activity (*SI Appendix*, Fig. S2*A*). To compensate for the loss of function, we increased the induction of MgrB C16A W20C (pTrc promoter with 10 μM IPTG), which ensured significant repression of PhoQ during cross-linking (*SI Appendix*, Fig. S2*D*). Additionally, a FLAG tag was fused to the N terminus of MgrB (*SI Appendix*, Fig. S2*E*) to facilitate the detection of the PhoQ/MgrB complex in Western blot. Cu-phenanthroline was added to the cells to catalyze the disulfide formation between sulfhydryl groups at a close distance. When MgrB C16A W20C was coexpressed with PhoQ Y32C, we observed a higher-molecular-weight band at around 55 kDa on the Western blot corresponding to the PhoQ/MgrB complex (Fig. 1*D* and *SI Appendix*, Fig. S3*A*). This band was reduced by the addition of dithiothreitol (DTT) and was absent when the cysteine residue was at position 16 (WT), or no cysteine was in the MgrB transmembrane helix (C16A). The results are consistent with our prediction, suggesting the close proximity of MgrB W20 with the PhoQ TM1 residue Y32 in the complex. Additionally, we found that PhoQ L204C cross-linked with MgrB W20C, indicating position 20 near L204 in PhoQ TM2 as well (Fig. 1*D* and *SI Appendix*, Fig. S3*A*). Furthermore, we tested PhoQ Cys variants in the neighboring positions of 32 and 204 (PhoQ 31C, 33C, 203C, and 205C). None of the variants formed detectable cross-linked complexes with MgrB W20C in the western blot (*SI Appendix*, Fig. S2*G*). Functionally, PhoQ L204C partially restored the MgrB W20C inhibition. PhoQ Y32C restored it to a lesser extent, which is probably due to the large difference between Tyr and Cys side chains as well as the relatively buried location of Y32 (*SI Appendix*, Fig. S2*F*). Taken together, our results suggest that MgrB W20 interacts with residue Y32 in PhoQ TM1 and L204 in PhoQ TM2.

Using MgrB residue 20 as a reference point, we next identified interacting amino acids of two more functionally important residues (Q22 and F24) in the MgrB TM helix (30). In both cases, we observed stronger cross-linking bands and more than one cross-linked position in both transmembrane helices of PhoQ (Fig. 1 *E* and *F* and *SI Appendix*, Fig. S3 *B* and *C*). For MgrB

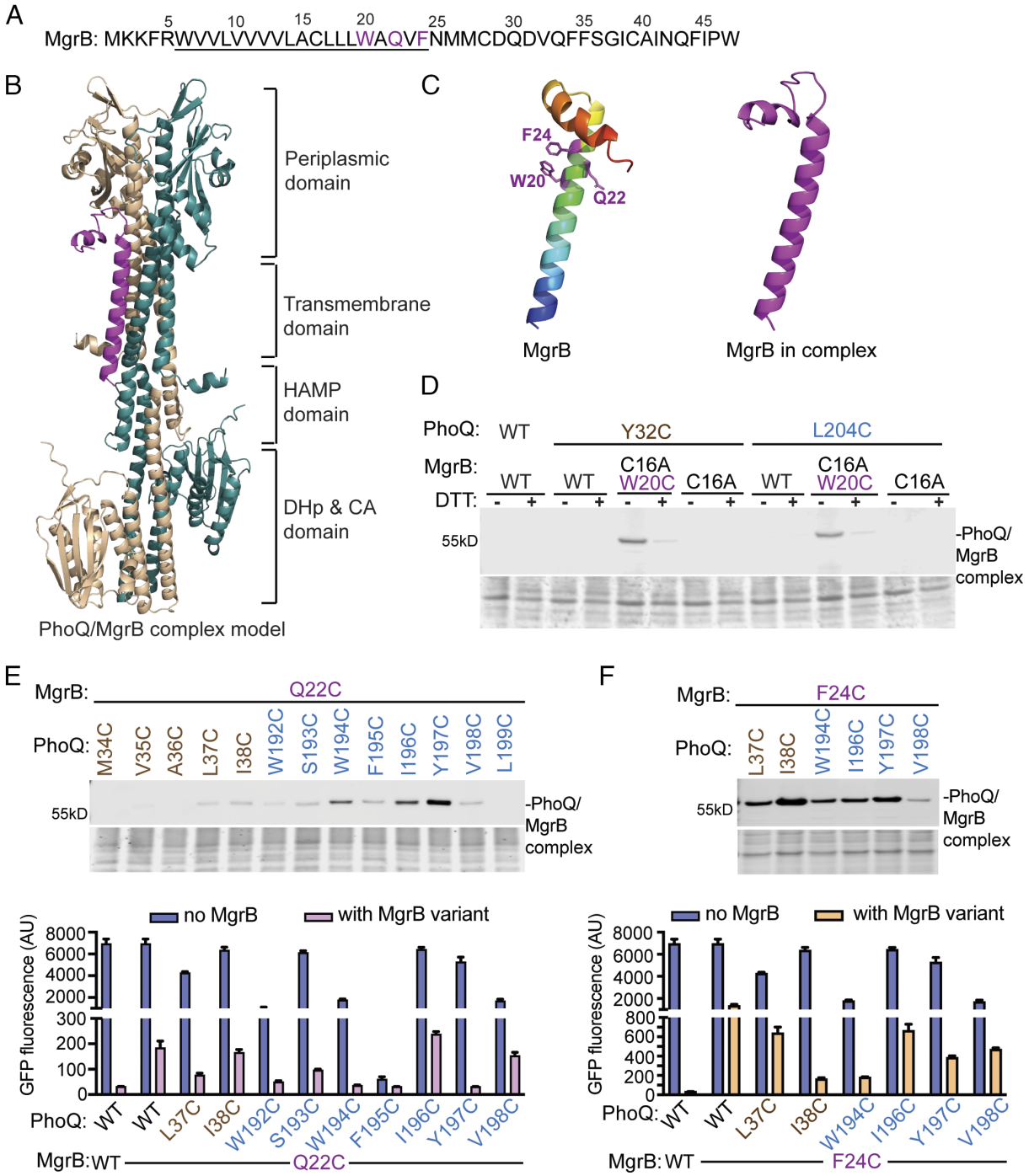

Fig. 1. Identification of the interacting residues between MgrB and PhoQ in the transmembrane helices. (*A*) The sequence of MgrB from *E. coli*. Residues predicted to be in the transmembrane helix are underlined. (*B*) The tertiary structure of the top-ranked PhoQ/MgrB complex predicted by AlphaFold2. The two PhoQ protomers are colored in wheat and teal. MgrB is colored in magenta. (*C*) The structural models of MgrB predicted by AlphaFold2 are shown in the ribbon. The model of MgrB alone (*Left*) is colored in the rainbow spectrum with the N terminus in blue and the C terminus in red. The positions involved in cross-linking (20, 22, and 24) are in purple and shown with side chains in ball-and-stick. The predicted structure of MgrB in complex (*Right*) is colored in magenta. All structural figures were prepared using PyMOL unless otherwise stated. (*D*, *E* Top, *F* Top) Western blot analysis of *E. coli* membrane extracts after disulfide cross-linking. The indicated PhoQ and FLAG-tagged MgrB variants were expressed in *E. coli*, followed by Cu-phenanthroline catalyzed disulfide cross-linking (details in *Materials and Methods*). The total protein stain of the PVDF membranes serves as loading control. Residues from PhoQ TM1 and TM2 are colored in wheat and teal, respectively. Magenta indicates the residues in the MgrB TM helix. Data are representative of at least three independent experiments. (*D* bottom, *F* bottom) The functional assay of PhoQ Cys-variants with or without MgrB. A GFP reporter plasmid carrying the *gfp* gene fused with a PhoP-regulated promoter P_{mgtLA} was introduced to the *E. coli* strain. The expression of *phoQ* and *mgrB* variants was induced, and cells were grown to the early log phase. The function of PhoQ variants was then monitored by measuring the GFP fluorescence of the cell culture. Each data point is shown with the calculated average and SD from three independent biological replicates.

Q22C, stronger cross-links were observed to residues in the PhoQ TM2 helix (colored blue). The strongest cross-linking band was shown when PhoQ Y197C was coexpressed. The cross-linking efficiency decreased when the cysteine residue moved to the neighboring positions and further away (196C, 195C, and 198C). It was then partially recovered when the cysteine (194C) was roughly one helical turn away from Y197 (Fig. 1*E*). Functionally, the Y197C mutation in PhoQ restored the MgrB Q22C activity

Table 1. The Cα-Cα distance of cross-linked residue pairs in the PhoQ/MgrB structural model

Cα-Cα distance (Å)	W20-Y32	W20-L204	Q22-Y197	F24-I38
Model 1	12.10	12.80	8.30	9.10
Model 2	12.90	11.90	9.60	10.80
Model 3	12.90	10.10	10.00	11.30
Model 4	13.60	11.90	10.20	11.40
Model 5	14.20	16.40	16.20	11.60

the best when compared to other PhoQ TM_Cys mutants, supporting the notion that MgrB Q22 primarily interacts with PhoQ Y197.

For MgrB F24C (Fig. 1*F* and *SI Appendix*, Fig. S3*C*), the strongest cross-linking was found with a PhoQ TM1 mutant, I38C. Functionally, PhoQ I38C showed the highest extent of activity reduction when coexpressed with MgrB F24C, thus restoring the activity of MgrB F24C the best among the tested PhoQ/MgrB pairs. The minor cross-linking events observed could be due to the greater distance between the cysteine residues or an indication of intermediate binding states of MgrB. Notably, one PhoQ Cys variant, F195C, retained only about 1% of the wild-type activity (Fig. 1*E*). Mutants with such a severe functional defect may have altered MgrB binding, thus unsuitable for the cross-linking approach. For other PhoQ variants in Fig. 1 *E* and *F*, some showed moderately reduced activity, possibly due to the reduced protein expression level (i.e., PhoQ W192C in *SI Appendix*, Fig. S3*F*). More importantly, the presence of MgrB significantly repressed the activity of these PhoQ variants, indicating that the change caused by cysteine substitutions does not have a major impact on MgrB inhibition.

Collectively, we identified four-pair residues of MgrB and PhoQ located in close proximity at the protein interface of the complex: W20-Y32, W20-L204, Q22-Y197, and F24-I38. In the AlphaFold2 predicted complex models, these cross-linked pairs were positioned less than 14 Å in the top four ranked models (Table 1). Furthermore, Q22-Y197 and F24-I38 had shorter Cα-Cα distances than the W20-Y32 and W20-L204 pairs, consistent with our experimental results where the former two pairs showed higher cross-linking efficiency.

Cross-Linking in the Periplasmic Domains of PhoQ and MgrB. To gain insights into PhoQ/MgrB interactions at the periplasmic domains, we attempted to identify interacting residue pairs using site-specific photo-cross-linking (35). We introduced an amber stop codon at each residue in the MgrB periplasmic region (residues 25 to 47). The photo-cross-linking amino acid, *p*-benzoyl-l-phenylalanine (*p*Bpa), was then incorporated into the flag-tagged MgrB at the amber stop codon via the orthogonal $tRNA^{Amber}$ and the aminoacyl-tRNA synthetase in *E. coli*. After UV irradiation, we detected bands with a molecular weight of ~55 kDa by anti-FLAG antibody when *p*Bpa was incorporated at positions 26, 30, 32, and 38, indicating the formation of the UV-dependent cross-linked PhoQ/MgrB complex (Fig. 2*A* and *SI Appendix*, Fig. S4).

The cross-linked products from positions 30, 32, and 38 could be purified and subjected to mass spectrometry (MS) analysis (*SI Appendix*, Fig. S4 and Dataset S1). PhoQ was detected in all samples as the most prominent protein. Only a small number of other proteins were identified, indicating that the protein purification steps were highly effective. MgrB was challenging to detect due to its small size, high hydrophobicity, and a low number of potential MS-detectable peptides. However, we increased the sample injection amount, which allowed for the successful identification of MgrB in cross-linked complex samples, except when *p*Bpa was incorporated at position 38. This was most likely due to the interference of the digestion step with the incorporated *p*Bpa. Despite the successful identification of both PhoQ and MgrB in the cross-linked samples, confident MS identification of MgrB-PhoQ cross-linked peptides providing clear evidence toward positioning the two proteins in the complex was not possible. The lack of cross-linked products with other *mgrB_amber* constructs (*SI Appendix*, Fig. S4) could be due to the low efficiency of *p*Bpa incorporation (i.e., position 29) and/or the obstruction of the bulky unnatural amino acid on the binding of MgrB to PhoQ. Most of the residues that resulted in cross-linked products were within the MgrB C28-C39 loop region, suggesting its possible direct interaction with PhoQ.

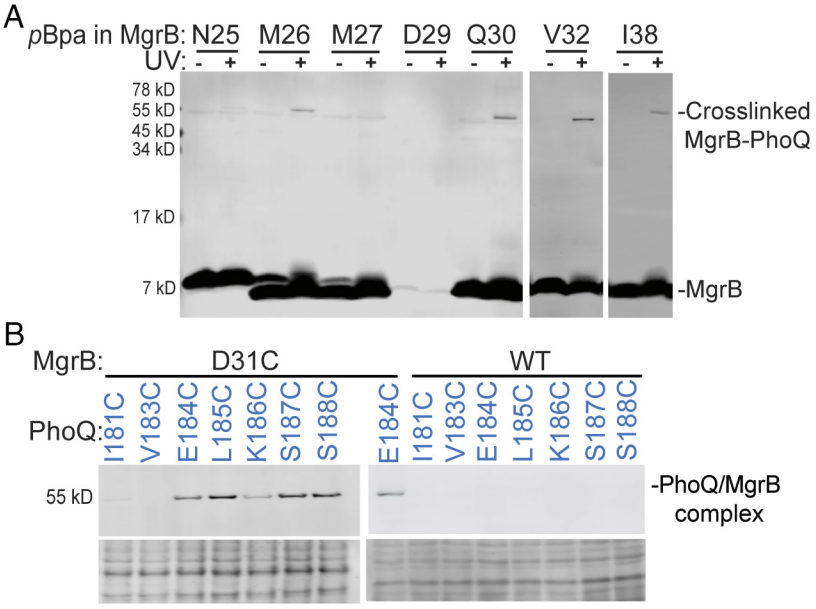

Fig. 2. Site-specific photo cross-linking in the periplasmic domain. (*A*) Western blot analysis of the site-specific photo cross-linking between PhoQ and MgrB. The *E. coli ΔphoQΔmgrB* strain harboring pETduet-1 *phoQ-his*$_6$ *flag-mgrB* and pEVOL-pBpF vectors was grown in LB containing the unnatural amino acid, *p*Bpa, which was incorporated into the FLAG-tagged MgrB at the indicated positions via the amber stop codon and the cognate tRNA/aminoacyl-tRNA synthetase pair. Cells were treated with UV light. The cross-linked MgrB-PhoQ complex was detected with western blot using antibodies directed to the FLAG epitopes. Samples without UV irradiation served as controls. (*B*) Western blot analysis of disulfide cross-linking from MgrB residue 31 to the PhoQ linker region connecting the periplasmic domain to the TM2 helix. The experimental procedure is as in Fig. 1*D*, and details can be found in *Materials and Methods*. Data are representative of at least three independent experiments.

In the AlphaFold2 complex model, the MgrB C28-C39 loop was close to the PhoQ linker region connecting the periplasmic and the TM domains. To test whether the MgrB C28-C39 loop interacts directly with the linker region, we performed disulfide cross-linking with MgrB D31C and PhoQ_linker_Cys variants. Due to the presence of two essential cysteines in the MgrB periplasmic region, we first tested whether introducing a third cysteine would affect MgrB function. We observed that the introduction of a third cysteine at position 31 did not reduce MgrB inhibition as much as the single cysteine variant, C39A (*SI Appendix*, Fig. S5), suggesting that the cysteine at position 31 does not severely interfere with the C28-C39 disulfide bond formation. Therefore, MgrB D31C is suitable for cross-linking experiments. The cross-linking results showed that MgrB 31C formed disulfide linkages with cysteines in several positions in the PhoQ linker region (184 to 188) with a similar amount of cross-linked complex (Fig. 2*B* and *SI Appendix*, Fig. S3*D*). No cross-linked products were detectable in the control sample, where the wild-type MgrB (C28 and C39) was coexpressed with PhoQ_linker_Cys mutants (Fig. 2*B* and *SI Appendix*, Fig. S3*E*). Our data thus support that MgrB D31 interacts with the PhoQ linker region. The comparable amount of cross-linked complex at multiple positions is probably due to the flexible nature of the MgrB C28-C39 loop.

The Conformational Change of the PhoQ Linker Region upon MgrB Binding. After mapping the MgrB binding site on PhoQ, we next sought to detect MgrB-induced PhoQ conformational change by comparing the PhoQ dimer cross-linking pattern with MgrB to the one without MgrB. For the PhoQ linker region, we focused on residues 187 and 188, which showed different conformations in PhoQ monomer and dimer models (*SI Appendix*, Fig. S6*A*). These two residues were located at the periplasmic end of the TM2 helix and at a similar lateral position as the TM1 residue 43 (*SI Appendix*, Fig. S6*B*). By monitoring the cross-linking efficiency between residues at positions 43 and 188, we intended to detect local helical movements upon MgrB binding. In the absence of MgrB, we observed that 43C and 188C formed an intramolecular disulfide linkage, manifesting as a faster-migrating band below the PhoQ monomer band (Fig. 3*A*). DTT treatment of the same sample retarded the migration to the exact location as the PhoQ monomer, excluding the likelihood of protein degradation. Nearly no PhoQ dimer band was detected under this condition, further supporting that the orientation of the 188C side chain was more toward the TM1 helix of the same protomer. In the presence of MgrB, the cross-linking pattern changed. The intramolecular cross-linking band reduced, and the intensity of the PhoQ dimer band increased (Fig. 3*A* and *SI Appendix*, Fig. S6*C*). In this case, cross-linked PhoQ dimer could be formed in four ways: 43C-43'C, 43C-188'C, 43'C-188C, and 188C-188'C. Our control samples showed that the cross-linking was reduced for 43C-43'C and 188C-188'C when MgrB was present. Therefore, the increase in PhoQ dimer formation was likely due to the intermonomeric cross-linking between positions 43 and 188, suggesting that the binding of MgrB changes the cross-linking pattern from intra- to intermonomeric linkage and likely the relative orientation between PhoQ residue 188 to residue 43 (Fig. 3*B*). We also observed a

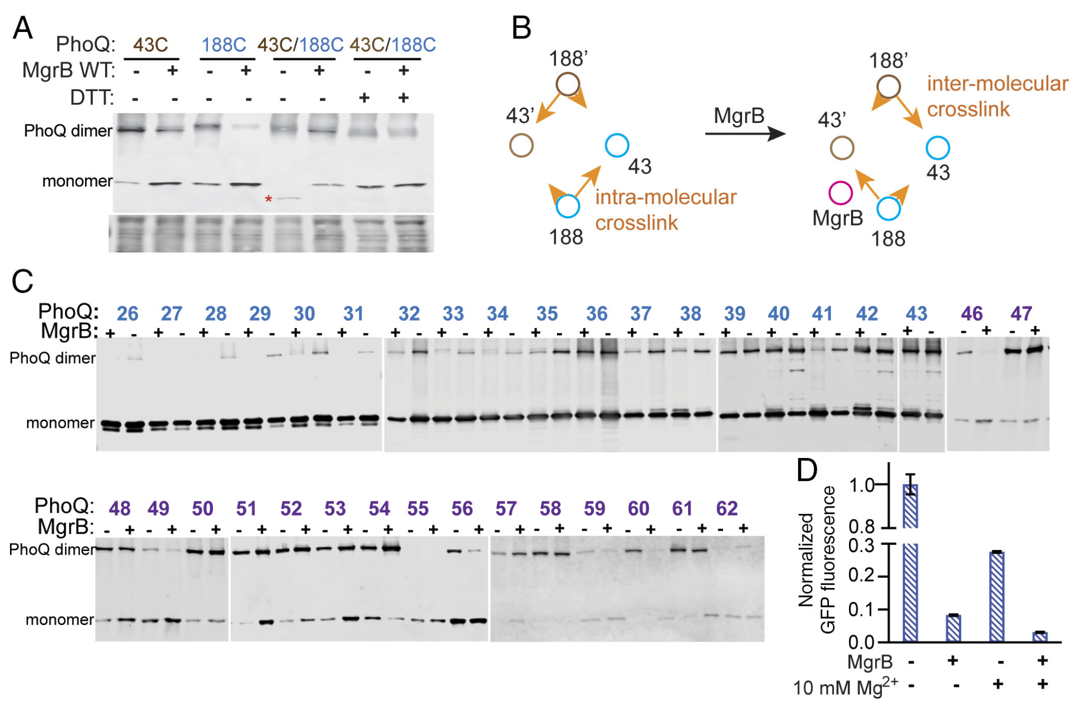

Fig. 3. The conformational change of the PhoQ sensor kinase upon MgrB binding. (*A*) Western blot analysis of disulfide cross-linking within the PhoQ molecule in the presence or absence of MgrB. The His_6-tagged PhoQ cysteine variants were expressed with or without the wild-type MgrB in *E. coli*. The disulfide cross-linking reaction was initiated with Cu-phenanthroline. The resulting cross-linked PhoQ species was then detected using Western blot with an anti-His antibody. The red asterisk indicates PhoQ molecules with an intramolecular disulfide cross-link. The total protein stain serves as a loading control. Data are representative of three independent experiments. (*B*) A diagram of MgrB affecting the disulfide cross-linking between the cysteine residues at positions 43 and 188. Brown and cyan circles represent the TM helices in each PhoQ monomer. The magenta circle represents MgrB. Orange arrows indicate the cross-linking tendency of Cys188 to Cys43 in the same or different PhoQ monomer. (*C*) MgrB induced PhoQ conformational change along the PhoQ dimer interface. The His_6-tagged PhoQ cysteine variants were expressed with or without the wild-type MgrB in *E. coli*. The experimental procedure is as described in A and details can be found in *Materials and Methods*. The position of cysteine is indicated as residue numbers in the PhoQ N-terminal helix. Numbers colored in blue and purple are residues in TM and periplasmic domains, respectively. Data are representative of three independent experiments. (*D*) The repression of PhoQ activity by high magnesium and MgrB. The activity of PhoQ was monitored with the GFP reporter system using the *E. coli* Δ*phoQ*Δ*mgrB* strain as described in Fig. 1*E*. Data are representative of three independent experiments. Each data point is shown with the calculated average and SD from three biological replicates.

similar trend of change in cross-linking for the residue 43 and 187 pair but with reduced intramolecular cross-linking efficiency (*SI Appendix*, Fig. S6*C*). Taken together, we hypothesize that MgrB may promote a rotational or translational movement of one TM2 periplasmic terminus toward the TM1 from the other protomer. Because the stoichiometry of PhoQ and MgrB remains unknown, further investigations would be needed to determine whether the conformational change detected here occurs in both PhoQ protomers.

MgrB Repression of PhoQ Is Divergent from High Magnesium Repression. Besides the small protein MgrB, high magnesium also represses PhoQ kinase activity (14). The structural change of PhoQ under magnesium repression was studied in detail by monitoring the arrangement of α helices along the PhoQ dimer interface via disulfide cross-linking (36). It was proposed that under high magnesium conditions, the N-terminal α helix across the TM and the periplasmic domains undergoes a scissoring-type of motion with the pivot point near the periplasm/membrane interface (36).

Using a similar approach, we monitored the arrangement of α helices along the PhoQ dimer interface in the presence and absence of MgrB. Our data showed that most TM1 residues had reduced cross-linking between PhoQ protomers upon MgrB binding (Fig. 3*C* blue residues, *SI Appendix*, Fig. S7). This reduction was more prominent for residues close to the cytoplasm, suggesting that MgrB binding pushes TM1-TM1' apart and the propagation of PhoQ conformational change from the periplasm to the cytoplasm. In contrast, the presence of MgrB did not show a similar cross-linking effect on residues along the periplasmic helical interface (Fig. 3*C* purple residues, *SI Appendix*, Fig. S7). Most residues in this region showed little change in the cross-linking pattern. Some showed a significantly decreased (i.e., residues 46 and 60) or a slightly increased dimer fraction (i.e., residues 62). The overall PhoQ dimer rearrangement upon MgrB binding differed from the scissoring motion proposed for high magnesium repression, suggesting that MgrB and high magnesium act differently on PhoQ. We then did functional analyses of PhoQ under high magnesium, with MgrB, or with both repressive factors. The results showed that PhoQ was further repressed significantly when both high magnesium and MgrB were present (Fig. 3*D*), supporting the hypothesis that magnesium and MgrB may have divergent mechanisms of repression.

Molecular Dynamics Simulations of PhoQ/MgrB Complex Models. When comparing the predicted PhoQ dimer with its complex with MgrB, there was only minor conformational change, which is in stark contrast to our experimental results. The AlphaFold2 prediction might have only captured a transient arrangement of the complex but not the final state. To investigate the effect of MgrB on the conformation of PhoQ in silico, we carried out a set of four molecular dynamic simulations. The initial atomic models were obtained using the best-ranked model predicted with the multimeric version of AlphaFold2. In total, we modeled four different complexes: PhoQ dimer i) alone and interacting with ii) the wild-type MgrB, iii) MgrB W20Y, and iv) MgrB W20A. Each complex was inserted into a bacterial mimetic membrane bilayer, and simulations were carried out up to 1 μs under near-physiological conditions. To evaluate the impact of the starting conformation on the stability of the PhoQ/MgrB complex, we carried out two additional 500 ns simulations seeded from the second and third predictions. All protein complexes remained stable throughout the entire simulations, with minor fluctuation in the secondary structure. We did not observe any significant differences between the three PhoQ/MgrB simulations. The MgrB C-terminal short helix (A40-W47) was buried close to the membrane surface. The C-terminal carboxylate group interacted with the head group of PE lipids in the simulations. The orientation of this C-terminal helix was primarily restrained by the disulfide linkage (C28-C39) and remained stable in the simulations. A principal component analysis (PCA) of the transmembrane domain clearly showed that the functional MgrB variants (WT and W20Y) induced a similar conformational change (Fig. 4*A*), corresponding to an increase in the distance between PhoQ TM1 helices, coupled with a decrease in distance between TM2 helices. This change is more evident in TM residues near the membrane/cytoplasm interface (Fig. 4*B* and *SI Appendix*, Fig. S8). The MgrB W20A had only a marginal impact on the conformation of the transmembrane domain.

In all the simulations with MgrB variants, we also observed the translocation of one of the PhoQ catalytic-ATP binding (CA) domains (Fig. 4*C*). This is most evident in the 1 μs simulations with the wild-type MgrB, where one CA domain moved fully away from the helix harboring the phosphorylatable histidine and located itself close to the inner membrane. For PhoQ alone, we did not observe any significant movement of the CA domains throughout the entire simulation. The functionally impaired MgrB W20A also induced PhoQ CA domain movement, though to a lesser extent compared to the wild type (Fig. 4*C*). In this simulation, the CA domain remained close to its initial position but rotated by about 90°. Our previous work showed that the W20A mutant had low activity due to reduced affinity to PhoQ (30). However, since the simulation was seeded with a complex where MgrB W20A was already interacting with PhoQ, this likely represents the scenario where overexpression of MgrB W20A compensates for its weak binding to PhoQ and partially recovers its inhibitory function.

Overall, the simulation results confirm our experimental observations, showing the PhoQ structural changes at the MgrB binding site. Furthermore, MgrB induces movements of the distantly located CA domain, suggesting that the local conformational change due to MgrB binding results in the repression of PhoQ kinase activity.

MgrB Mediates PhoQ Sensing CAMPs. Our cross-linking data (Fig. 2*B*) suggested that MgrB directly interacts with PhoQ E184, a residue involved in CAMP sensing (9). We, therefore, hypothesized that MgrB might affect PhoQ activation by CAMPs. To investigate this as well as the impact of MgrB on PhoQ sensing other stimuli, we tested PhoQ activation by CAMPs, low pH, and high osmolarity in the presence and absence of MgrB (Fig. 5). Under a repressive magnesium condition (LB medium supplemented with 10 mM Mg^{2+}), only slight or no PhoQ activation was detected by antimicrobial peptide C18G regardless of MgrB, consistent with previous work where high magnesium repressed the activation of PhoQ by CAMPs in *Salmonella* (9, 10). Conversely, with the same magnesium condition (10 mM), a relatively large activation of PhoQ was detected by low pH or osmolarity upshift in the presence of MgrB. The activation did not appear to have a qualitative change when MgrB was absent, except that the overall PhoQ activity increased due to the lack of MgrB repression (Fig. 5*A*).

We next followed PhoQ activities in the presence of antimicrobial peptide LL37 and C18G under a physiologically relevant magnesium concentration (1 mM Mg^{2+} in LB) that does not repress CAMPs from inducing PhoQ activity (9). Up to a nearly five-fold increase of PhoQ activity by antimicrobial peptides was detected when the wild-type MgrB was present (Fig. 5*B*). However, in the absence of MgrB, there was no significant further increase of PhoQ

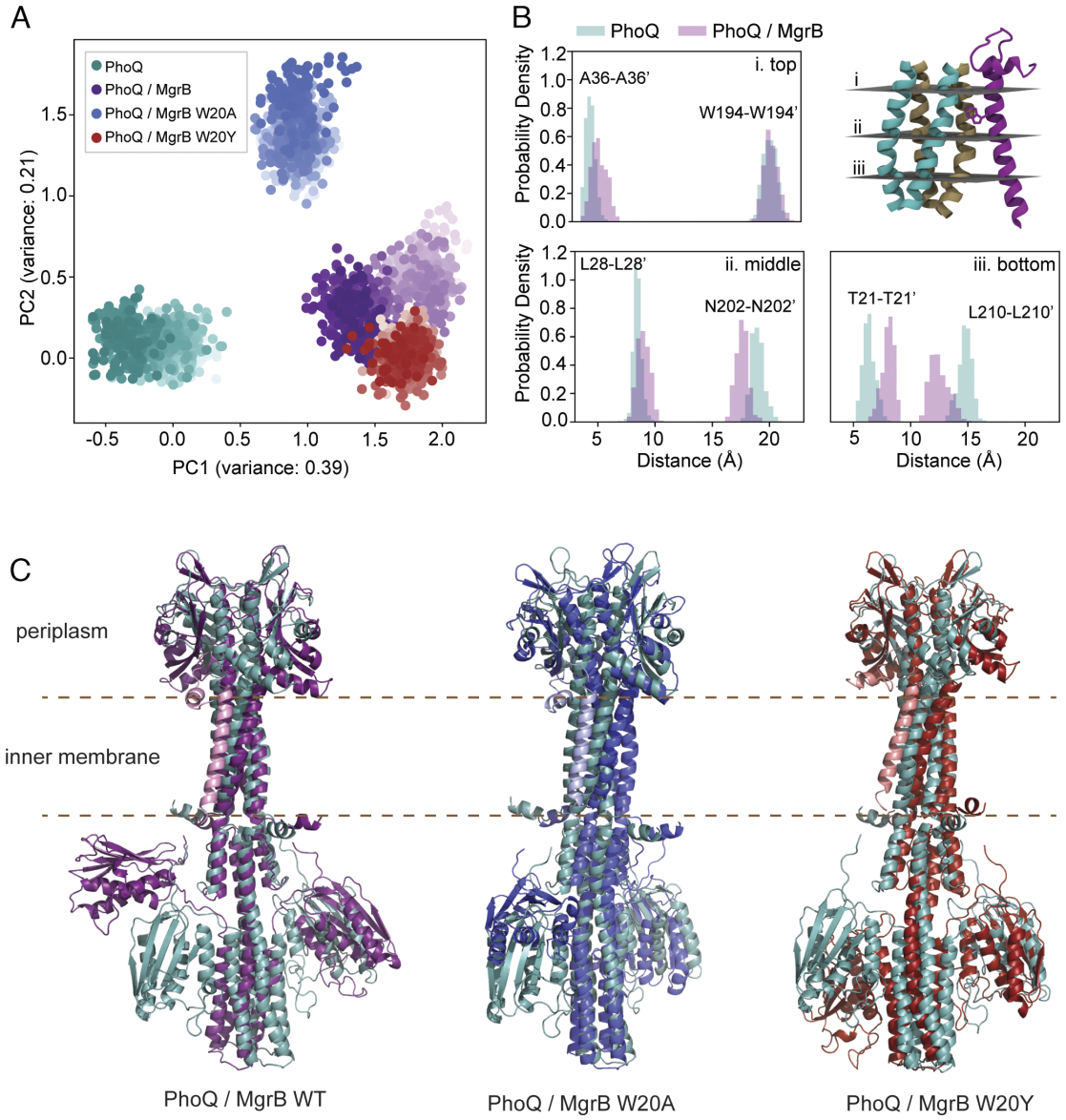

Fig. 4. Molecular dynamics simulations of PhoQ/MgrB complex models. (*A*) Projection of the molecular dynamics simulations into the eigenspace formed by the first two components of a PCA of the transmembrane domain of PhoQ (residues 21 to 38 and 194 to 215). Each point corresponds to a conformation of the TM and is colored in shades of teal, purple, red, and blue, for the simulations of PhoQ alone, and in complex with MgrB, MgrB W20Y, and W20A, respectively. Lighter shades correspond to conformations sampled earlier in the simulation. (*B*) Distribution in distances between TM1 – TM1' (*Left*) and TM2 – TM2' (*Right*) at the top, middle, and bottom of the PhoQ TM domain. (*C*) The overlay of the final conformations of PhoQ/MgrB complex models with the PhoQ dimer. PhoQ structures are colored as in *A*. The MgrB wild-type, W20A, and W20Y variants are colored in pink, light blue, and light red, respectively.

activity in the presence of C18G. In the case of LL37, only a marginal increase (1.14-fold) of PhoQ activity was observed, consistent with a previous report (15), suggesting that LL37 may be slightly different from C18G in terms of PhoQ activation. To test whether PhoQ was already maximally activated in the *ΔmgrB* strain with 1 mM magnesium, we treated the cells with additional stimuli. PhoQ activity was significantly further increased by lowered pH or elevated osmolarity (*SI Appendix*, Fig. S9*A*), indicating that PhoQ activity did not reach saturation with 1 mM magnesium alone. To be precise on the total magnesium concentration in the growth medium, we tested our strains in the defined minimal A medium (37) supplemented with 1 mM magnesium. Consistent with what we observed in LB, PhoQ activity was higher in the absence of MgrB but could not be further increased by C18G. Therefore, we hypothesize that MgrB may mediate PhoQ to sense antimicrobial peptides under a physiologically relevant magnesium concentration.

The lack of PhoQ activation by antimicrobial peptides in the absence of MgrB might also be due to the protective effect of the overall elevated activity of the PhoQ/PhoP two-component system, which could increase the outer membrane modification and reduce the entry of antimicrobial peptides to the periplasm. To obtain more direct evidence, we monitored PhoQ and MgrB interactions in vivo using the acceptor photobleaching Förster resonance energy transfer (FRET) approach. Functional PhoQ-mNeonGreen and mCherry-MgrB fusion proteins (*SI Appendix*, Fig. S9 *C* and *D*) were expressed in *E. coli*. Cells were collected in the mid-log phase, treated with C18G, and then used for FRET measurements (Fig. 5*C*). The control cells without C18G treatment or treated with nonfunctional peptides (the 3× FLAG peptide and a randomly scrambled C18G derivative) showed energy transfer from mNeonGreen to mCherry with about 10% efficiency (Fig. 5*C* and *SI Appendix*, Fig. S10), comparable to our previous report (12),

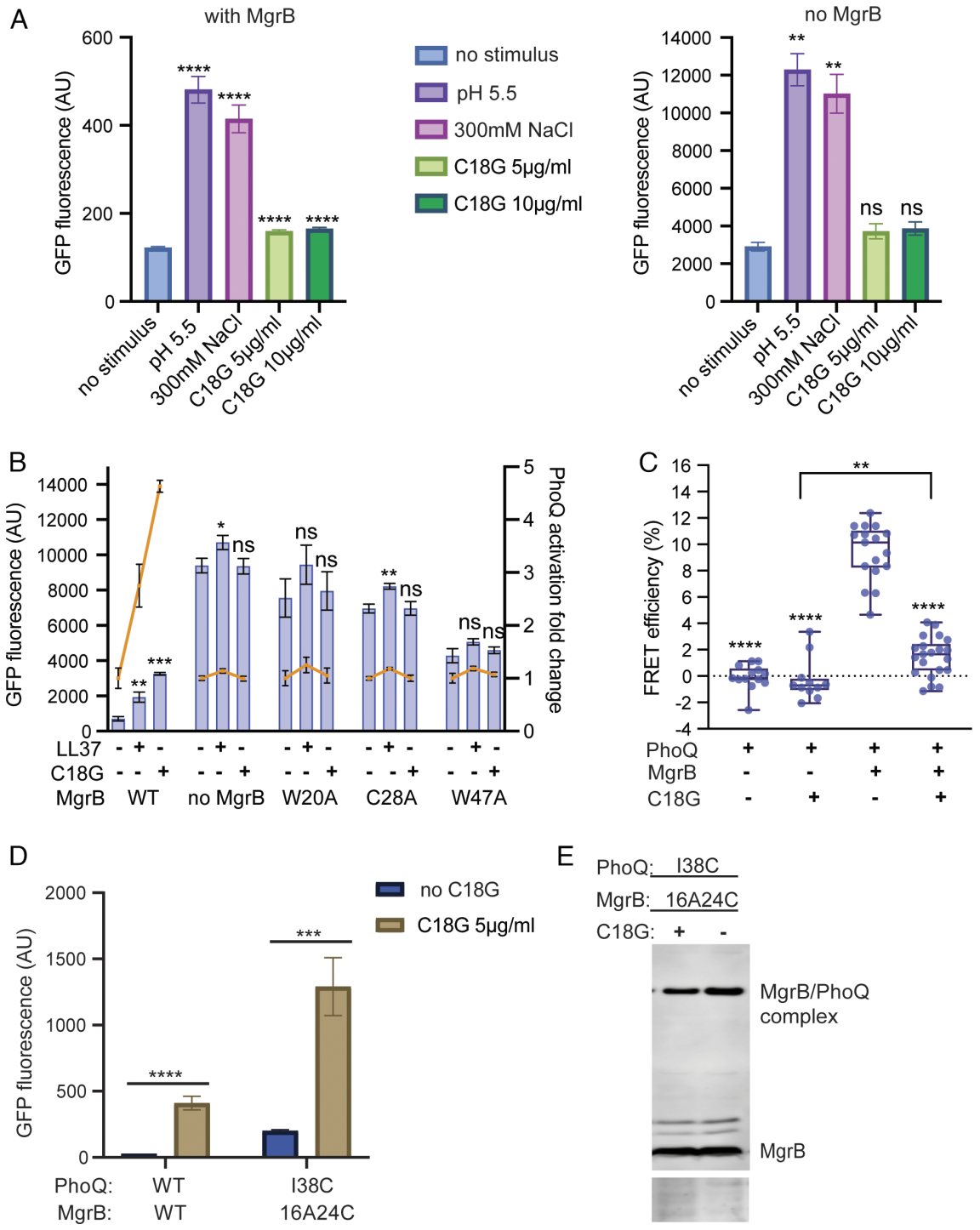

Fig. 5. The impact of MgrB on PhoQ sensing external stimuli. (*A*) The PhoQ activation in the presence or absence of MgrB under high magnesium conditions. *E. coli* MG1655 *ΔmgrB* strain harboring pBAD33 with (*Left*) or without (*Right*) *mgrB* gene was induced with arabinose and grown in the presence of indicated stimuli in LB media supplemented with 10 mM magnesium. The activity of PhoQ was monitored using the GFP reporter as described in Fig. 1*E*. (*B*) The activation of PhoQ in the presence of antimicrobial peptides and MgrB under 1 mM magnesium conditions. The orange lines indicate the fold change of PhoQ activity in the presence of antimicrobial peptides. *E. coli* MG1655 *ΔmgrB* strain expressing MgrB variants were grown in LB supplemented with 1 mM magnesium and antimicrobial peptides, LL37 (5 μg/mL) or C18G (5 μg/mL) as indicated. The PhoQ activity was followed as in *A*. (*C*) The FRET measurements of PhoQ-mNeonGreen and mCherry-MgrB in vivo. *E. coli* cells expressing PhoQ-mNeonGreen and mCherry-MgrB from plasmids were grown to mid-log phase and then treated with or without the antimicrobial peptide, C18G (10 μg/mL). The energy transfer from mNeonGreen to mCherry was then measured for each condition. The strains expressing no FRET receptor (mCherry-MgrB) serve as negative controls. (*D*) The activation of PhoQ variants in the presence of MgrB and C18G (5 μg/mL). The growth and induction conditions for the PhoQ and MgrB variants were the same as described before (Fig. 1 *F*, *Bottom*). The PhoQ activity was monitored by measuring the GFP reporter fluorescence. (*E*) Western blot analysis of PhoQ I38C MgrB 16A24C disulfide cross-linking in the presence or absence of C18G (5 g/mL). The cross-linking and Western blot experiments were performed as described before (Fig. 1 *F*, *Top*). The total protein stain of the membrane serves as a loading control. Data are representative of three independent experiments. Each data point in *A*–*D* is shown with the calculated average and SD from at least three independent experiments.The *P* value is represented by asterisk symbols and calculated using GraphPad Prism 9 software (*, $P \le 0.05$; **, $P \le 0.01$; ***, $P \le 0.001$; ****, $P \le 0.0001$; ns, not significant, $P > 0.05$).

indicating the formation of the PhoQ/MgrB complex in vivo. With the C18G treatment, the FRET efficiency reduced to about 2%, slightly higher than the negative controls, suggesting that C18G induces the dissociation of the PhoQ/MgrB complex.

To confirm the in vivo FRET results, we performed disulfide cross-linking experiments with or without C18G using the PhoQ I38C MgrB F24C variant pair. We chose this pair because i) they formed a good amount of PhoQ/MgrB cross-linked complex readily detectable by Western blot (Fig. 1*F*); ii) PhoQ I38C showed wild-type-like activity (Fig. 1*F*); iii) MgrB F24C repressed PhoQ I38C to a relatively low level (Fig. 1*F*); and iv) the variant pair responded to C18G showing significantly increased PhoQ activity (Fig. 5*D*). Compared to the cross-linking in the absence of C18G, we observed a lighter band corresponding to the PhoQ/MgrB complex (Fig. 5*E*). Quantification of the bands in the Western blot showed that the cross-linking efficiency between PhoQ and MgrB reduced from 46.4 to 32.7% in the presence of C18G. With the negative control peptides, such a reduction in cross-linking was not observed (*SI Appendix*, Fig. S10). Collectively, our data suggest that C18G induces MgrB to move away from PhoQ, consistent with our FRET results.

Taken together, we propose that MgrB is involved in PhoQ sensing CAMPs. Under physiologically relevant magnesium conditions, PhoQ is active but partially repressed due to the bound MgrB. This state allows PhoQ to detect and respond sensitively to CAMPs at a subinhibitory concentration. CAMPs bind to PhoQ and induce the release of the bound MgrB, further activating PhoQ/PhoP-regulated genes and potentially increasing bacterial resistance to CAMPs (Fig. 6).

Discussion

In this study, we report that MgrB directly interacts with the TM helices and the periplasmic/TM linker region of PhoQ, changing its conformation in a way that is divergent from high magnesium repression. It reduces the overall activity of PhoQ yet still allows its activation by low magnesium, low pH, and increased osmolarity. We further reveal that PhoQ activation by CAMPs is MgrB-dependent under physiologically relevant magnesium conditions. Our in vivo FRET and cross-linking data support that CAMPs induce MgrB dissociating from PhoQ and thus increase PhoQ activity via derepression. A higher PhoQ activity leads to an increased outer membrane modification and improved resistance to CAMPs. Since the septum is the initial attacking site of certain CAMPs (i.e., LL37) on the membrane (38), the possible division block caused by strong PhoQ activation may also protect bacteria against the host's innate immune response. CAMPs were suggested to bind to an acidic surface in the PhoQ periplasmic domain, although the exact binding site has not been well defined (9). The acidic cluster (^{148}EDDDDAE), a major component of the acidic surface, is relatively distant from the MgrB binding site. However, it remains unclear whether the acidic residue E184 in the linker region is directly involved in CAMP binding. It is plausible that the binding of CAMPs induces PhoQ conformational change, which leads to the dissociation of MgrB from PhoQ.

We observed that a high level of magnesium (10 mM) repressed PhoQ activation by CAMPs in the presence or absence of MgrB in *E. coli*. Under physiologically relevant magnesium conditions (1 mM), we observed PhoQ activation by CAMPs only in the presence of functional MgrB. These results are consistent with a previous report on PhoQ in *Salmonella* (having a chromosomal *mgrB*), even though MgrB had not yet been identified at that time (9). The same report proposed that CAMPs activate PhoQ by replacing magnesium ions from the acidic cluster in PhoQ, which is different from our MgrB-mediated CAMP sensing mechanism. Both hypotheses, however, do not necessarily conflict with each other but rather describe two aspects of PhoQ sensing CAMPs. It is also possible that magnesium may affect MgrB binding to PhoQ, thus connecting these two sensing mechanisms. Interestingly, the magnesium replacement mechanism cannot explain PhoQ activation by antimicrobial peptides in some cases. For example, a recent study revealed that antimicrobial peptides with a β-sheet structure or a neutral charge could also activate PhoQ (39). These atypical PhoQ activators do not possess the properties to interact with the PhoQ acidic cluster. Furthermore, there are PhoQ homologs that do not contain an acidic cluster in their sequences. Our MgrB-dependent antimicrobial peptide sensing mechanism could provide a suitable explanation for these cases.

By monitoring PhoQ conformational change and activities, we show that MgrB repression diverges from high magnesium repression. This is consistent with the different binding sites of magnesium and MgrB on PhoQ. Magnesium was suggested to bind to

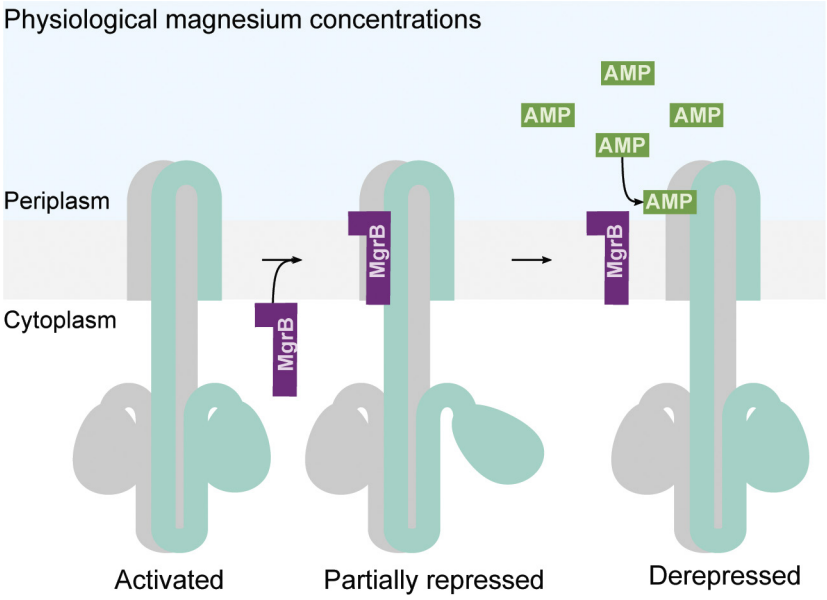

Fig. 6. The schematic representation of MgrB-mediated PhoQ activation by antimicrobial peptides. PhoQ is active under physiological magnesium conditions, inducing the expression of *mgrB*. The expressed MgrB binds to PhoQ, resulting in a partially repressed state. Antimicrobial peptides (AMPs) enter into the bacterial periplasm, bind to PhoQ, and cause MgrB to dissociate from PhoQ.

several locations, including the acidic cluster near the inner membrane (148 to 152) and residues G93, W97, H120, and T156 (14, 23, 40). Mutations of these residues were shown to abolish magnesium protection from iron-mediated protein cleavage (40). The majority of these residues are located in the peripheral of the periplasmic domain, distinct from the MgrB binding site.

Our cross-linking results revealed extensive interactions between MgrB and the PhoQ linker region, implying its importance in functional regulations. Highly conserved and functionally important residues are found in or near this region, such as K186, T48, R50, E184, and L185, mutations of which lead to alterations in PhoQ activity as well as signaling capability (20, 23, 24). Curiously, the wild-type MgrB maintained its inhibition on PhoQ linker variants, suggesting that the flexible MgrB loop may have various interaction modes with the PhoQ linker region. Interestingly, the PhoQ activating protein, SafA, appears to act near this linker region in terms of the putative SafA binding site, and the activation required intermonomeric salt bridge (R50'-D179) (41, 42). Whether MgrB repression competes with SafA activation of PhoQ and how these regulations are coordinated await further studies.

Sensor kinases in bacterial two-component systems are evolutionarily related and have structural resemblance. We found that the predicted structures of EnvZ, QseC, and CreC sensor kinases closely resemble the PhoQ structure. EnvZ was also shown to form a complex with MgrB experimentally (30). With the mechanism of MgrB revealed here, it is foreseeable that small protein regulators can be designed for PhoQ, EnvZ, and possibly many other sensor kinases. This will contribute to the repertoire of unconventional antimicrobial agents targeting sensor kinases that regulate bacterial virulence (43) and to the treatment of infections caused by drug-resistant pathogens.

Materials and Methods

Bacterial Strains, Plasmids, and Growth Conditions. The complete lists of strains, plasmids, and primers used in this study are summarized in *SI Appendix*, Tables S1–S3, respectively. The *E. coli* MG1655 *ΔmgrB* and *ΔphoQΔmgrB* strains were from the previous study (30). All strains were grown in the lysogeny broth (LB) medium or minimal A medium (37) containing 0.2% glycerol, 0.1% casamino acids supplemented with magnesium as indicated. Cells were grown at 37 °C with shaking unless otherwise indicated. Genes in the pTrc99a vector were induced with isopropyl β-D-1-thiogalactopyranoside (IPTG) at a final concentration of 10 μM. Genes in the pBAD vector were induced with 0.008% arabinose. Genes in the pEVOL-pBpF vector were induced with 0.02% arabinose. Genes in the pETduet-1 vector were induced with IPTG at a final concentration of 0.5 mM. When appropriate, the antibiotics ampicillin, kanamycin, and chloramphenicol were used at concentrations of 100 μg/mL, 50 μg/mL, and 34 μg/mL, respectively. A detailed description of cloning and plasmid construction can be found in *SI Appendix, Materials and Methods*.

Disulfide Cross-Linking In Vivo. The in vivo disulfide-cross-linking experiments were performed as previously described with modifications (44). Briefly, cells carrying pBAD33 *phoQ* variant and pTrc99A *mgrB* variant were grown at 37 °C in LB medium supplemented with 10 mM $MgSO_4$ overnight, then diluted 1:100 to fresh LB medium supplemented with 1 mM $MgSO_4$. The expression of plasmid-encoded proteins was induced with arabinose and IPTG. When the OD_{600} value reached 0.6, cells were harvested, washed, and resuspended in the cross-linking buffer (137 mM NaCl, 2.7 mM KCl, 10 mM Na_2HPO_4, 1.8 mM KH_2PO_4, 1 mM $MgSO_4$, and 0.1 mM Cu-phenanthroline), followed by 10 min incubation at 25 °C. The reaction was stopped by pelleting the cells and then resuspending in the 1× stop-solution (8 mM sodium phosphate buffer, pH 7.8, 12.5 mM EDTA, and 12.5 mM N-ethylmaleimide) and incubation at 25 °C for 10 min. Cells were collected, resuspended in the lysis buffer (50 mM Tris–HCl, pH 8.0, 100 mM NaCl, and protease inhibitors), mixed with lysing matrix B beads (MP Biomedicals), and broken with a homogenizer following the manufacturer's instructions. The mixture was spun down at 2,300× g for 10 min at 4 °C to pellet the beads and cell debris. The supernatant was centrifuged at 21,000× g for 1 h at 4 °C to pellet the membrane fraction, which was then dissolved in the SDS sample buffer at 4 °C overnight. The membrane proteins were separated on an SDS tris–tricine or tris–glycine polyacrylamide gel via electrophoresis and analyzed with western blot.

Western Blot Analysis. Proteins were transferred from a polyacrylamide gel to a polyvinylidene fluoride membrane or nitrocellulose membrane. PhoQ-His and Flag-MgrB were detected with the anti-His and anti-Flag primary antibodies (Sigma), respectively. The IRDye 800CW-conjugated secondary antibody (LI-COR) was used, and the protein bands were visualized with the Odyssey CLx imaging system (LI-COR) and quantified with ImageJ. The cross-linking efficiency was calculated by dividing the amount of PhoQ/MgrB complex with the total amount of PhoQ/MgrB complex and MgrB monomer.

Functional Assay with the *gfp* Reporter Gene. The GFP reporter assay was performed as a previous study with modifications (12). Briefly, the reporter plasmid pUA66 P_{mgtLA}-*gfp* (12) was transformed to strains indicated. The resulting transformants were grown overnight at 37 °C in LB or minimal A medium with indicated $MgSO_4$ and then diluted 1:100 to fresh medium with magnesium and/or stimuli as indicated. The cultures were grown at 37 °C with vigorous shaking till the early log phase (OD = 0.4 to 0.5). The fluorescence of cells was monitored with a BD LSRFortessa SORP flow cytometer (BD Biosciences) equipped with a 100-mW 488-nm laser and a 510/20 bandpass filter. BD FACSDiva software version 8.0 (BD Biosciences) was used to analyze the acquired data.

Unnatural Amino Acid Incorporation in MgrB and Site-Specific UV Cross-Linking In Vivo. The site-specific photo-cross-linking experiments were performed as in previous studies with modifications (35, 45). *E. coli* BL21 DE3 cells carrying pETduet-1 *phoQ-his*$_6$ *flag-mgrB* and pEVOL-pBpF vectors were grown in LB medium at 37 °C overnight and then diluted 1:100 to fresh LB medium containing 0.5 mM *p*Bpa. When the OD_{600} value reached around 0.6, cells were induced with arabinose (0.02%) and IPTG (0.5 mM) for 4h at 30 °C, followed by harvesting, washing two times, and resuspension in 1 mL cold PBS buffer. The bacterial suspension was spread out onto a 35-mm round dish on ice and irradiated for 5 min with 365 nm UV light using an LED UV hand lamp (Honle UV technology). Cells were then harvested at 4 °C, and the formation of cross-linked PhoQ/MgrB complex was then detected by the separation of total protein with polyacrylamide gel electrophoresis and western blot with anti-Flag antibody. The cross-linked complex was purified by affinity chromatography, separated in an sodium dodecyl sulfate polyacrylamide gel, and verified by mass spectrometry (see *SI Appendix, Materials and Methods* for details).

Molecular Modeling and Molecular Dynamics Simulations. The PhoQ/MgrB complex was modeled using AlphaFold2 multimer on Colab [PMID: 35637307]. We considered six different complexes: i) PhoQ, ii) PhoQ/MgrB (predictions ranked 1 to 3), iii) PhoQ/MgrB W20Y variant, and iv) PhoQ/MgrB W20A variant. Each complex was inserted into a bacterial membrane mimetic composed of a mixture of phosphatidylethanolamine and phosphatidylglycerol with a 3:1 ratio. The systems were solvated with a 17 Å water padding and neutralized with NaCl at a concentration of 150 mM. Each system was assembled using the CHARMM-GUI web server (46).

The simulation was performed with the CHARMM36m force field, including CMAP corrections for the protein (47). The water molecules were described with the TIP3P water parameterization (48). The simulations were carried out with OPENMM molecular engine (49) following the minimization and equilibration protocols provided by CHARMM-GUI. The cutoff for nonbonded interactions was set to 12 Å with a switching distance at 10 Å. The periodic electrostatic interactions were computed using particle-mesh Ewald summation. A constant temperature of 310 K was imposed by Langevin dynamics with a damping coefficient of 1.0 ps. The constant pressure of 1 atm was maintained with Monte Carlo barostat (50). The hydrogen mass repartitioning scheme was used to achieve a 4-fs time step (51). Each simulation was carried out up to 1 μs and up to 500 ns for the second- and third-ranked predictions of PhoQ/MgrB.

Acceptor Photobleaching FRET Analysis. FRET measurements were performed as described before (30). The expression of PhoQ-mNeonGreen and mCherry-MgrB was induced in *E. coli* lptD4213 strain with 0.008% arabinose

and 10 μM IPTG, respectively. The cultures were grown to the mid-log phase (OD = 0.6) in LB media. Cells were harvested and washed twice with prechilled tethering buffer (20 mM potassium phosphate pH 7.0, 1 μM methionine, and 10 mM lactic acid). The surface of a glass-bottom 96-well plate (Greiner) was treated with 0.1% poly-L-lysine for 15 min at room temperature, followed by removing poly-L-Lysine and air-drying for 5 min. The wells were washed twice using a prechilled tethering buffer. Subsequently, cells were incubated in the wells at room temperature for 25 min to allow attachment. Unattached cells were removed by washing with tethering buffer twice, and attached cells were overlaid with tethering buffer with or without 10 μg/mL C18G and incubated at room temperature for 1 h. Acceptor photobleaching FRET was performed using the same microscope settings as published previously (30). The details of the data acquisition and analysis can be found in *SI Appendix, Materials and Methods*.

Data, Materials, and Software Availability. All study data are included in the article and/or supporting information.

ACKNOWLEDGMENTS. We thank L. Cassidy and A. Throley (the Christian-Albrecht University of Kiel) for performing mass spectrometry analyses and writing and editing the manuscript; H. Koch (the Albert Ludwig University of Freiburg) for pEVOL-pBpF vector and the site-directed photo-cross-linking protocol; M. Stopp for the disulfide cross-linking protocol; S.G. Sierra for technical assistance; and members of the Yuan and the Sourjik laboratories for helpful discussions. We thank G. Storz (NIH), V. Sourjik (Max Planck Institute for Terrestrial Microbiology), R. Lill (Philipps University of Marburg), and S. Yadavalli (Rutgers University) for their suggestions to improve the manuscript. This work is supported by the German Research Foundation (DFG) priority program 2002 YU 247/3-1 and the Max Planck Society (to J.Y.) and the Swiss National Science Foundation grant PCEFP3_194606 (to T.L. and S.L.).

1. M. Duval, P. Cossart, Small bacterial and phagic proteins: An updated view on a rapidly moving field. *Curr. Opin. Microbiol.* **39**, 81–88 (2017).
2. K. S. Ramamurthi, G. Storz, The small protein floodgates are opening; now the functional analysis begins. *BMC Biol.* **12**, 96 (2014).
3. M. Su *et al.*, Small proteins: Untapped area of potential biological importance. *Front. Genet.* **4**, 286 (2013).
4. K. Weidenbach *et al.*, Small proteins in archaea, a mainly unexplored world. *J. Bacteriol.* **204**, e00313–21 (2022).
5. H. Sberro *et al.*, Large-scale analyses of human microbiomes reveal thousands of small, novel genes. *Cell* **178**, 1245–1259.e14 (2019).
6. M. R. Hemm, J. Weaver, G. Storz, *Escherichia coli* small proteome. *EcoSal. Plus* **9,** 10.1128/ecosalplus.ESP-0031-2019 (2020).
7. S. S. Yadavalli, J. Yuan, Bacterial small membrane proteins: The swiss army knife of regulators at the lipid bilayer. *J. Bacteriol.* **204**, e0034421 (2022).
8. E. A. Groisman, A. Duprey, J. Choi, How the PhoP/PhoQ system controls virulence and Mg(2+) homeostasis: Lessons in signal transduction, pathogenesis, physiology, and evolution. *Microbiol. Mol. Biol. Rev.* **85**, e0017620 (2021).
9. M. W. Bader *et al.*, Recognition of antimicrobial peptides by a bacterial sensor kinase. *Cell* **122**, 461–472 (2005).
10. L. R. Prost *et al.*, Activation of the bacterial sensor kinase PhoQ by acidic pH. *Mol. Cell* **26**, 165–174 (2007).
11. J. Choi, E. A. Groisman, Acidic pH sensing in the bacterial cytoplasm is required for *Salmonella* virulence. *Mol. Microbiol.* **101**, 1024–1038 (2016).
12. J. Yuan, F. Jin, T. Glatter, V. Sourjik, Osmosensing by the bacterial PhoQ/PhoP two-component system. *Proc. Natl. Acad. Sci. U.S.A.* **114**, E10792–E10798 (2017).
13. M. A. Carabajal *et al.*, PhoQ is an unsaturated fatty acid receptor that fine-tunes *Salmonella* pathogenic traits. *Sci. Signal* **13**, eaaz3334 (2020).
14. E. Garcia Vescovi, F. C. Soncini, E. A. Groisman, Mg^{2+} as an extracellular signal: Environmental regulation of *Salmonella* virulence. *Cell* **84**, 165–174 (1996).
15. A. M. Lippa, M. Goulian, Feedback inhibition in the PhoQ/PhoP signaling system by a membrane peptide. *PLoS Genet.* **5**, e1000788 (2009).
16. Y. Eguchi *et al.*, B1500, a small membrane protein, connects the two-component systems EvgS/EvgA and PhoQ/PhoP in *Escherichia coli*. *Proc. Natl. Acad. Sci. U.S.A.* **104**, 18712–18717 (2007).
17. S. S. Yadavalli *et al.*, Antimicrobial peptides trigger a division block in *Escherichia coli* through stimulation of a signalling system. *Nat. Commun.* **7**, 12340 (2016).
18. Y. Eguchi *et al.*, Regulation of acid resistance by connectors of two-component signal transduction systems in *Escherichia coli*. *J. Bacteriol.* **193**, 1222–1228 (2011).
19. H. Salvail, J. Choi, E. A. Groisman, Differential synthesis of novel small protein times *Salmonella* virulence program. *PLoS Genet.* **18**, e1010074 (2022).
20. S. Sanowar, A. Martel, H. L. Moual, Mutational analysis of the residue at position 48 in the *Salmonella enterica* Serovar Typhimurium PhoQ sensor kinase. *J. Bacteriol.* **185**, 1935–1941 (2003).
21. A. G. Regelmann *et al.*, Mutational analysis of the *Escherichia coli* PhoQ sensor kinase: Differences with the *Salmonella enterica* serovar Typhimurium PhoQ protein and in the mechanism of Mg^{2+} and Ca^{2+} sensing. *J. Bacteriol.* **184**, 5468–5478 (2002).
22. S. Minagawa *et al.*, Isolation and molecular characterization of the locked-on mutant of Mg^{2+} sensor PhoQ in *Escherichia coli*. *Biosci. Biotechnol. Biochem.* **69**, 1281–1287 (2005).
23. U. S. Cho *et al.*, Metal bridges between the PhoQ sensor domain and the membrane regulate transmembrane signaling. *J. Mol. Biol.* **356**, 1193–1206 (2006).
24. J. Cheung *et al.*, Crystal structure of a functional dimer of the PhoQ sensor domain. *J. Biol. Chem.* **283**, 13762–13770 (2008).
25. C. D. Waldburger, R. T. Sauer, Signal detection by the PhoQ sensor-transmitter. Characterization of the sensor domain and a response-impaired mutant that identifies ligand-binding determinants. *J. Biol. Chem.* **271**, 26630–26636 (1996).
26. E. S. Venturini *et al.*, A global data-driven census of *Salmonella* small proteins and their potential functions in bacterial virulence. *microLife* **1**, uqaa002 (2020).
27. A. M. S. Shein *et al.*, High prevalence of *mgrB*-mediated colistin resistance among carbapenem-resistant *Klebsiella pneumoniae* is associated with biofilm formation, and can be overcome by colistin-EDTA combination therapy. *Sci. Rep.* **12**, 12939 (2022).
28. M. E. Salazar, A. I. Podgornaia, M. T. Laub, The small membrane protein MgrB regulates PhoQ bifunctionality to control PhoP target gene expression dynamics. *Mol. Microbiol.* **102**, 430–445 (2016).
29. A. M. Lippa, M. Goulian, Perturbation of the oxidizing environment of the periplasm stimulates the PhoQ/PhoP system in *Escherichia coli*. *J. Bacteriol.* **194**, 1457–1463 (2012).
30. S. S. Yadavalli *et al.*, Functional determinants of a small protein controlling a broadly conserved bacterial sensor kinase. *J. Bacteriol.* **202**, e00305–20 (2020).
31. M. Mirdita *et al.*, ColabFold: Making protein folding accessible to all. *Nat. Methods* **19**, 679–682 (2022).
32. R. Evans *et al.*, Protein complex prediction with AlphaFold-Multimer. bioRxiv [Preprint] (2022). https://doi.org/10.1101/2021.10.04.463034 (Accessed 4 October 2021).
33. M. Akdel *et al.*, A structural biology community assessment of AlphaFold2 applications. *Nat. Struct. Mol. Biol.* **29**, 1056–1067 (2022).
34. H. U. Ferris *et al.*, Mechanism of regulation of receptor histidine kinases. *Structure* **20**, 56–66 (2012).
35. Y. Ryu, P. G. Schultz, Efficient incorporation of unnatural amino acids into proteins in *Escherichia coli*. *Nat. Methods* **3**, 263–265 (2006).
36. K. S. Molnar *et al.*, Cys-scanning disulfide crosslinking and bayesian modeling probe the transmembrane signaling mechanism of the histidine kinase, PhoQ. *Structure* **22**, 1239–1251 (2014).
37. J. H. Miller, *A Short Course in Bacterial Genetics - A Laboratory Manual and Handbook for Escherichia coli and Related Bacteria* (Cold Spring Harbor Laboratory Press, 1992).
38. K. A. Sochacki *et al.*, Real-time attack on single *Escherichia coli* cells by the human antimicrobial peptide LL-37. *Proc. Natl. Acad. Sci. U.S.A.* **108**, E77–E81 (2011).
39. K. R. Brink *et al.*, An *E. coli* display method for characterization of peptide-sensor kinase interactions. *Nat. Chem. Biol.* **19**, 451–459 (2023).
40. S. Chamnongpol, M. Cromie, E. A. Groisman, Mg^{2+} sensing by the Mg^{2+} sensor PhoQ of *Salmonella enterica J. Mol. Biol.* **325**, 795–807 (2003).
41. Y. Eguchi *et al.*, The connector SafA interacts with the multi-sensing domain of PhoQ in *Escherichia coli*. *Mol. Microbiol.* **85**, 299–313 (2012).
42. K. Yoshitani *et al.*, Identification of an internal cavity in the PhoQ sensor domain for PhoQ activity and SafA-mediated control. *Biosci. Biotechnol. Biochem.* **83**, 684–694 (2019).
43. I. Cabezudo *et al.*, Effect-directed synthesis of PhoP/PhoQ inhibitors to regulate *Salmonella* virulence. *J. Agric. Food Chem.* **70**, 6755–6763 (2022).
44. M. Stopp *et al.*, Transmembrane signaling and cytoplasmic signal conversion by dimeric transmembrane helix 2 and a linker domain of the DcuS sensor kinase. *J. Biol. Chem.* **296**, 100148 (2021).
45. P. Kuhn *et al.*, Ribosome binding induces repositioning of the signal recognition particle receptor on the translocon. *J. Cell Biol.* **211**, 91–104 (2015).
46. S. Jo *et al.*, CHARMM-GUI: A web-based graphical user interface for CHARMM. *J. Comput. Chem.* **29**, 1859–1865 (2008).
47. R. B. Best *et al.*, Optimization of the additive CHARMM all-atom protein force field targeting improved sampling of the backbone phi, psi and side-chain chi(1) and chi(2) dihedral angles. *J. Chem. Theory Comput.* **8**, 3257–3273 (2012).
48. W. L. Jorgensen, J. Chandrasekhar, J. D. Madura, Comparison of simple potential functions for simulating liquid water. *J. Chem. Phys.* **79**, 926–935 (1983).
49. P. Eastman *et al.*, OpenMM 7: Rapid development of high performance algorithms for molecular dynamics. *PLoS Comput. Biol.* **13**, e1005659 (2017).
50. K. H. Chow, D. M. Ferguson, Isothermal-isobaric molecular dynamics simulations with Monte Carlo volume sampling. *Comp. Phys. Comm.* **91**, 283–289 (1995).
51. C. Balusek *et al.*, Accelerating membrane simulations with hydrogen mass repartitioning. *J. Chem. Theory Comput.* **15**, 4673–4686 (2019).